Reconstructing a 3D-Model from an Unregistered Range Image

Wu, Shin - Ting[1]
Rosana Marques da Silva[2]
Mercedes Rocío Gonzales Márquez[1]

[1] DCA – Faculty of Electrical and Computer Engeneering
State University of Campinas, 13081–970 São Paulo, Brazil
[2] DME – Science and Tecnology Center
Federal University of Paraiba, 58109–970 Paraíba, Brazil

11th April 2000

Abstract *In this paper we present yet another reconstruction technique which generates a 3D closed triangular mesh from an unregistered range image by deforming discretely an initial triangular mesh. Combining the advantages of the previous work on a deformable model and on a function-graph model, our algorithm avoids not only holes in the reconstructed surfaces, but also self-intersections as well.*

Keywords: Deformable models, range image, 3D closed mesh reconstruction.

1 Introduction

Despite a variety of published work, the 3D reconstruction from a set of range images is still a challenging and important problem for vision community. Since no single range image suffices to describe completely the surface of an object, additional methods were devised either to register multiple range images before surface model creation [10, 2] or to "zipper" multiple meshes reconstructed from unregistered range images [7]. In this context we may classify the known reconstruction techniques into three schemes: zippering approach, deformation approach, and volumetric approach.

In the "zippering" approach, meshes (usually triangular) are constructed from unregistered range images, and then they are "zippered" together to build a closed 3D surface model. The simplest way to build a mesh from an unregistered range image is to consider the range image as a sample of a graph-function. Hence, one may build a triangular mesh by connecting the adjacent points uniformly [7] or adaptatively [6]. Only the points on the depth border require special handling [7]. In the deformation approach, a 3D closed surface is obtained by deforming an initial shape estimated on the basis of the previously registered range data. And, in the volumetric approach [2], the underlying representation schema is indeed the spatial enumeration one, where the value of the signed distance function to the unknown surface is computed for each cell. Therefore, to obtain a 3D surface representation, conversion algorithms, such as a marching cube algorithm [8], are necessary (Figure 1).

Due to the data inaccuracy, the numerical imprecision during segmentation, and specially the occlusion problem, it is still a hard problem to integrate separately reconstructed meshes into a surface without "unwanted holes". Recent results on the volumetric approach show that filling holes in the spatial enumeration representation may be performed in a much

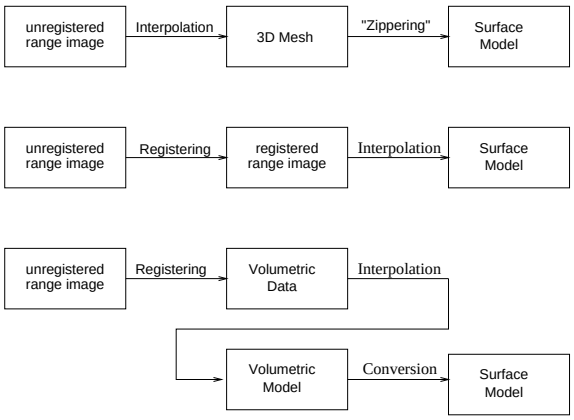

Figure 1: Different reconstruction approaches.

more natural way than in the surface (boundary) representation [2]. The deformation approach, however, has the advantage that there is no hole filling problem at all. This is the reason for attempting yet another deformation-based reconstruction algorithm. It is indeed an attempt to overcome the limitations presented in the discrete deformation approach and to make it competitive with the volumetric one (Figure 2).

Figure 2: An alternative reconstruction scheme.

The deformation process emulates indeed a physical behavior. An initial simple elastic object is subject to internal and external forces, estimated from images [3]. Governed by the continuous mechanical laws the object shape is dynamically deformed, until it reaches the equilibrium state. There are two research directions. One direction is to reduce the problem to a functional minimization one, whose objective-function is to fit the sampled (image) points with a minimal elastic energy surface [3, 4]. Therefore, the initial shape must be "similar" to the reconstructed model. Another direction is to reshape dynamically the initial model [10] in a discrete way. Instead of minimization, correspondence between the mesh vertices and the image data must be established during the growth process. The second technique has an advantage that it is not necessary to analyze the input data preliminarily to obtain the required deforming force, whereas the first one avoids self-intersections.

Our proposal is based on the *inflating balloon model* [10] with a number of modifications, namely improvement on the numerical robustness, on the usage of the available data, and on the restrictions on the initial estimate.

The paper is organized as follows. In section 2 we present the basic idea of our proposed *radial flow method*. Next, in section 3, some experimental results are given. Finally, in section 4 some concluding remarks are drawn.

2 Our proposal

From the range data the initial reference system is determined and an initial closed mesh $\mathcal{M}^0$ is placed on the origin of this reference system. Under the influence of a radial force, the mesh inflates as its vertices v_i move towards the corresponding point in the range image $\mathcal{R}$. When the length of an edge, v_iv_j in the mesh is greater than a specified tolerance d_{max}, it is subdivided and the mesh must be refined to maintain a triangular topology.

The sequence of operations refining–inflating is repeated, until no more subdivision and no more inflation is possible. Then, reconstruction errors are evaluated. If there are no faces in the mesh $\mathcal{M}^i$ with reconstruction errors, we consider that the aimed reconstructed 3D model is achieved. Otherwise, the triangular faces that still have reconstruction errors are grouped into disjoint sets of faces. These sets of faces are denoted fronts (of growth). From each of them we determine a new radial reference system before carrying out again the cyclic sequence refine–inflating to yield a new mesh $\mathcal{M}^{i+1}$ (Figure 3).

Note that the connections between vertices v_iv_j induce a planar graph on $\mathcal{R}$: the corresponding points of v_i and v_j define the nodes and the induced connections, the branches. Hence, for each face F in $\mathcal{M}^i$ there is a cor-

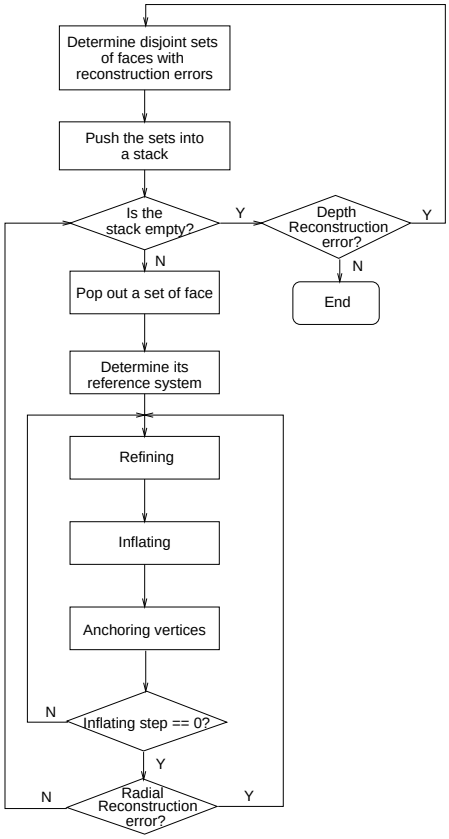

Figure 3: Our Proposal.

responding region $\mathcal{F}$ in $\mathcal{R}$ (Figure 4).

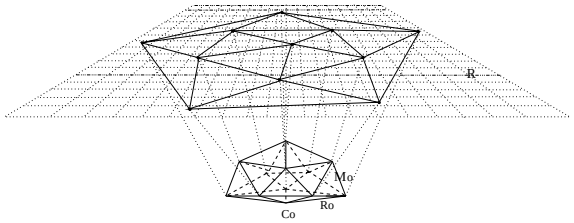

Figure 4: Correspondence model/image.

Our reconstruction method seems rather simple, but in its implementation we faced several problems:

1. how should we refine the mesh such that no self-intersections?

2. how should be the control of the growth step such that the reconstructed 3D-model does not cross the range data?

3. how should the reconstruction error be determined?

4. how should we compute conveniently each reference system?

5. how should the noise be handled?

The key operations in our algorithm are the search for a correspondence to a newly inserted vertex and the subdivision of a "triangle" with new inserted vertices in such a way that: (1) in each deforming front there is no ambiguous radial correspondence between its vertices and the corresponding points on an image and (2) each face is likely homeomorphic to its corresponding region.

Inspired by the triangulation on the range image that yields a 3D mesh without self-intersections [6, 2], we maintain the planarity of the induced graph in $\mathcal{R}$ at each iteration by looking for the corresponding sample point (to a newly inserted vertex on an edge) in the corresponding adjacent faces of the edge (Figure 5). Furthermore, our algorithm ensures

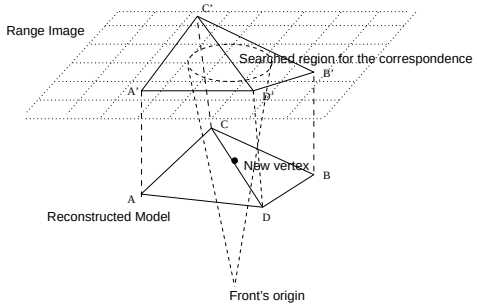

Figure 5: The search domain.

that the corresponding point lies in the "solid angle" defined by the bounding edges of these faces and the radial direction of this point intersects one of the two adjacent faces (Figure 6). To avoid unnecessary refinement, subdivisions on the faces and edges almost parallel to the radial growing direction are restricted.

The overgrowth of $\mathcal{M}^i$ is controlled by computing at each iteration the radial reconstruction error of the inflating face. The minimum of the radial reconstruction errors in each growing front is used as the growth step. The radial

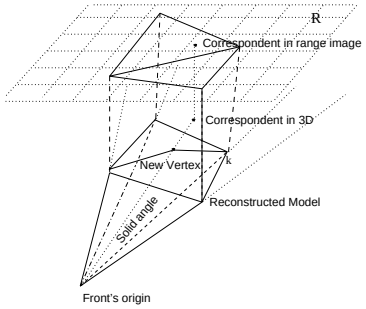

Figure 6: A solid angle.

reconstruction error is simply the radial distance of each sample point to the reconstructed model (Figure 7).

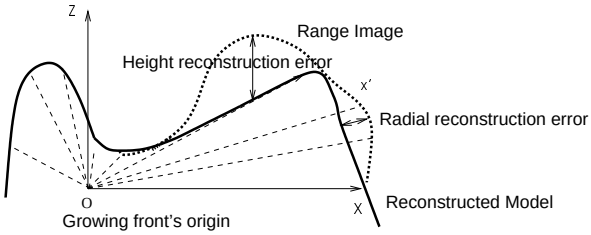

Figure 7: The radial and height reconstruction errors.

We distinguish two classes of reconstruction errors: radial and "height" reconstruction error. One refers to the reconstruction error in each growing front and the other to the reconstruction error relative to the "depth direction" of the range image. It is because that the radial growth strategy may yield degenerated growing directions when a set of vertices may move in the direction parallel to its adjacent triangles (Figure 7). It occurs frequently when the range image data are not from star-shaped objects. In this case, if no new growth fronts were created no inflation effect is produced and details may be missed.

The determination of each new radial growing direction is decisive on its successful growth. According to Chen and Medioni [10], if every sampled range points belonging to a front is within 45° of the reference system's z-axis, we have a favorable deformation. Therefore, we use for each front a reference system that has (1) its z-axis coincides with the direction from the point of interest in the reconstructed model to its corresponding point and (2) its origin on a point such that the vector of each image point belonging to the front is within 45° from z-axis (Figure 8). It is worth

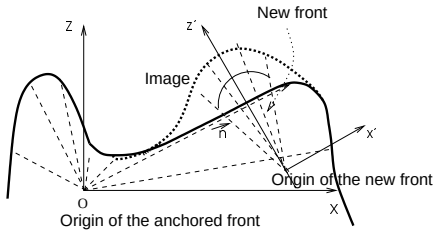

Figure 8: Reference system of a front.

mentioning that when we change the reference system of a front, the radial distance of each non-anchored vertex must be reevaluated to ensure a uniformly radial growing. After several experiments, we got satisfactory results when we used as the initial radial distance the minimal radial distance of the sampled image points on the regions corresponding the the adjacent faces of the vertex (Figure 9). In addi-

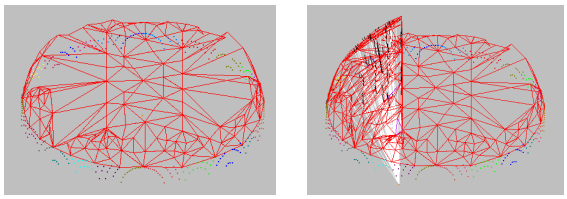

Figure 9: Reevaluation of radial distances.

tion, the new value of d_{max} must be recalculated to ensure new subdivisions.

For handling noise the surface tension strategy [10] is applied on the adjacent vertices that are not separated by the depth border. At each iteration the velocity of each vertex is weighted by its adjacent vertices and the reconstruction errors of its adjacent faces. We denominate this weight a stiffness factor. Hence, the geometry of the reconstructed model is not affected by an isolated noise (Figure 10).

3 Empirical evaluation

We have implemented our algorithm in C on a UNIX platform. It is runnable on SUN-

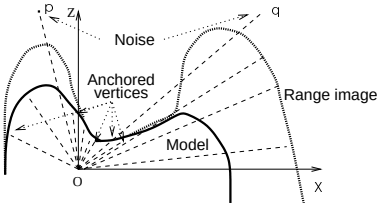

Figure 10: Noises.

SPARC, IBM-AIX, and PC (Linux).

TDM [9], Topological Data Model, library is used to manage our radial flow model. TDM provides its user a variety of functionalities to create, to manipulate, and to inquire the topology of an object, without knowing the underlying data structure. In our case, it not only ensures the topological consistency (new topological rearrangements) in each subdivision, but also helps in obtaining topological information, such as the oriented contours of a set of triangles and the neighboring data.

To demonstrate the performance of our algorithm in handling efficiently all the information contained in a range image, just one cartesian image was used for each reconstructed model.

For illustration, we include in this section the radial flow models reconstructed from 5 synthetic images and 4 real images. For each of them we present two data formats: input (range) data and the corresponding radial flow model rendered by Geomview [5].

We first tested the algorithm on the synthetic image of a cone (Figure 11). In this case,

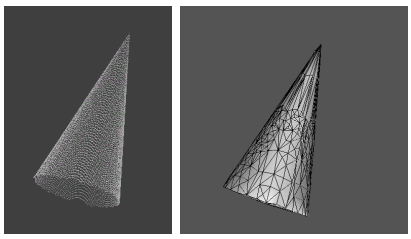

Figure 11: Cone.

we observed the combined action of d_{max} and stiffness factor. Surface tension acts against the growing force, reducing the velocity of the vertices towards the cone apex to zero. But, through the error determination, new growing fronts were detected and new value for d_{max} was determined to favor new subdivisions until the neighborhood of the cone apex was actually achieved.

Then, we tested the performance of our algorithm in handling discontinuities in the range data (Figure 12). In this case, the concept of

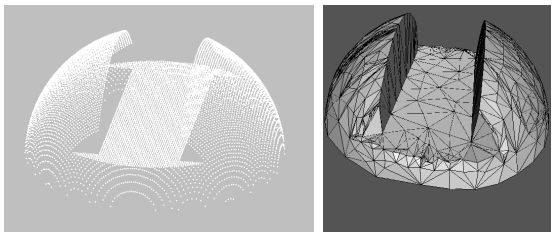

Figure 12: Esfcub.

solid angle was important for controlling the movement of a vertex towards ambiguous correspondences, which leads to the reconstruction of a "valley" in the object even though the range image does not contain the information about the occluding faces. Note that our radial model could not only reconstruct approximately the borderline of the discontinuities, but also "filled" the "missed" faces that should exist between these borders. Another challenging problem was the reconstruction of a "mountain" from a range image with several valleys (Figure 13). The concept of feasi-

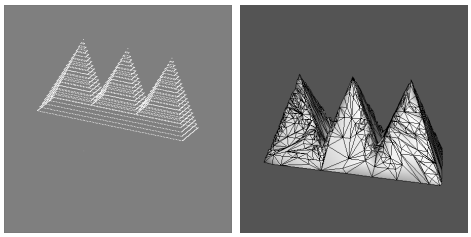

Figure 13: A mountain with three peaks.

ble searching domain for a corresponding point was decisive in the success of our algorithm.

For testing the adaptability of our algorithm with regard to the geometry of the reconstructed model, we use it to reconstruct a sphere and a plain face with distinct reconstruction error tolerances. Note that this tolerance only has influence on the triangular mesh

where the curvature is higher (Figure 14).

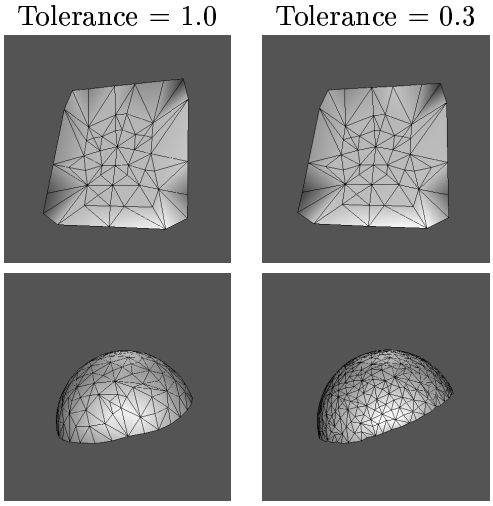

Figure 14: Adaptability.

In order to test our algorithm for complex objects, we reconstructed the real image data of Chopin bust (Figure 15), Mozart bust (Figure 16) and the Bigwye (Figure 17) taken from MSU/WSU range database [1]. In these cases, we experimented the capability of our algorithm for reconstructing a non-star shaped object and for avoiding self-intersections in the regions with closely spaced features.

Figure 15: Chopin's bust.

Finally, we experimented our algorithm for a part of the Chopin image data – only its head (Figure 18). The objective of this experiment was to compare the performance of our algorithm for star and non-star shaped objects. In this case, less growing iterations were used to reconstruct much more details.

Figure 16: Mozart's bust.

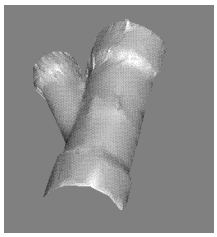

Figure 17: Bigwye.

Table 1 summarizes the number of vertices and the number of faces that we got for each reconstructed model with reconstruction error equal to 1.0 unit. We also included the number of growing fronts and the number of iterations that were needed.

4 Conclusions

We presented a new reconstruction algorithm for the complex objects. It is based on a local deformation approach, using a *radial flow model*. The feature for a reconstructed algorithm is its capability to utilize the most available data in each range image and yields a 3D mesh without self-intersections and "gaps" between two adjacent faces. Our algorithm can automatically infer the initial point and adapt the maximal allowed edge length and growing velocity in each front.

From our experiments, we can state that our reconstruction algorithm behave well for local surface properties, even when we deal with non-star shaped objects.

image	size (points)	vertices	faces	growing fronts	growing iterations
Cone	128×128 (12303)	642	1280	15	669
Esfcub	128×128 (12449)	782	1560	22	326
Mountain	128×128 (12449)	901	1798	39	307
Plane	128×128 (12449)	56	108	1	147
Hemisphere	128×128 (12449)	162	320	1	70
Chopin's Bust	356×232 (45191)	10113	20222	278	2292
Mozart's Bust	263×399 (61426)	7686	15368	211	1588
Head	131×142 (13026)	1697	3390	123	532
Bigwye	185×225 (21345)	1226	2448	56	976

Table 1: Summary of the experimental results.

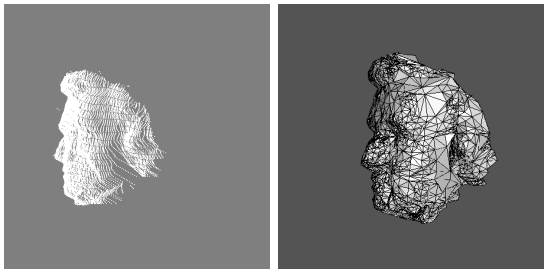

Figure 18: Chopin's head.

As further work, we intend to provide a mechanism that permits the reconstruction of an object that is not topologically equivalent to the initial mesh.

References

[1] Msu/wsu range database: Usc image (composer). http://www.eccs.wsu.edu.

[2] Brian Curless and Marc Levoy. A vlumetric method for building complex models from range images. In *Computer Graphics Proceedings*, pages 303–312, New Orleans, Louisiana, August 1996. SIGGRAPH 96.

[3] D.Terzopoulos, A.Witkin, and M.Kass. Constraints on deformable models: Recovering 3d shape and nonrigid motion. *Artificial Intelligence*, 38:91–123, 1988.

[4] D.Terzopoulos and D.Metaxas. Dynamic 3d models with local and global deformations: Deformable superquadrics. *IEEE Trans. on patt. Anal. Machine Intell*, 13(7):703–714, 1991.

[5] http://www.geom.umn.edu/software/download/geomview.html.

[6] H.T.Tanaka. Accuracy-based sampling and reconstruction whit adaptative meshes for parallel hierarchical triangulation. *Computer Vision and Image Understanding*, 61(3):335–350, 1995.

[7] Greg Turk and Marc Levoy. Zippered polygon meshes from range images. In *Computer Graphics Proceedings*, pages 311–318, Orlando, Florida, July 1994.

[8] W.E.Lorensen and H.E.Cline. Marching cubes: A high resolution 3d surface construction algo rithm. *ACM Computer Graphics*, 21(4):163–169, July 1987.

[9] Shin-Ting Wu. Non-manifold data models: Implementational issues. In *Proceedings of MICAD'92*, pages 38–56, Paris, França, 1992.

[10] Y.Chen and G.Medioni. Description of complex objects from multiple range images using an inflating balloon model. *Computer Vision and Image Understanding*, 1995.